ACS Photonics

Article

pubs.acs.org/journal/apchd5

Superlattice Plasmons in Hierarchical Au Nanoparticle Arrays

Danqing Wang,[†] Ankun Yang,[‡] Alexander J. Hryn,[‡] George C. Schatz,*[,†,§] and Teri W. Odom*[,†,‡,§]

[†]Graduate Program in Applied Physics, [‡]Department of Materials Science and Engineering, and [§]Department of Chemistry, Northwestern University, Evanston, Illinois 60208, United States

Supporting Information

ABSTRACT: Periodic metal nanoparticle (NP) arrays support narrow lattice plasmon resonances that can be tuned by changing the localized surface plasmons of the individual NPs in the array, NP periodicity, and dielectric environment. In this paper, we report superlattice plasmons that can be supported by hierarchical Au NP arrays, where finite arrays of NPs (patches) are organized into arrays with larger periodicities. We show that superlattice plasmons can be described by the coupling of single-patch lattice plasmons and Bragg modes defined by the patch periodicity. Superlattice plasmon resonances are often significantly narrower than that of single-patch lattice plasmon resonances and exhibit stronger local peak fields. By varying the periodicity of the patches, we demonstrated that the number and spectral location of superlattice plasmon resonances can be tailored in hierarchical Au NP arrays. These narrow superlattice plasmon resonances open prospects in ultrasensitive sensing and energy transfer and plasmon amplification in plasmonic cavities.

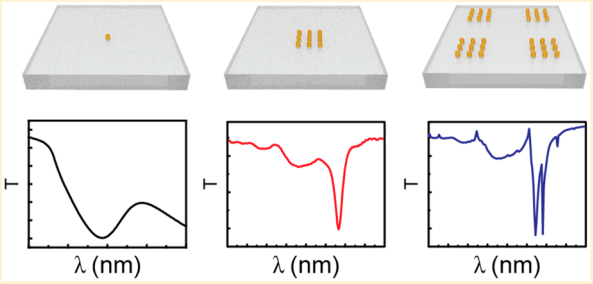

KEYWORDS: *superlattice, lattice plasmons, hierarchical, metal nanoparticles, Bragg modes, mode coupling*

Periodic arrays of metal nanoparticles (NPs) support lattice plasmons with narrow resonances when the localized surface plasmons (LSPs) of the constituent NPs couple with the Bragg modes of the lattice.[1−7] Lattice plasmons can be tuned by NP size and periodicity, where resonances as narrow as 4 nm full-width-at-half-maximum (fwhm) can be achieved.[6−8] For NP arrays with periodicities less than 1 μm, only first-order Bragg modes couple with the LSPs of the particles to generate the lattice plasmons.[2−4] Moreover, NP arrays with narrow lattice plasmon resonances (quality factors ∼ 100−200) can function as nanocavities for surface-emitting lasers.[8−11] By taking advantage of their sensitivity to dielectric environment,[12−17] we have shown that lattice plasmon lasers can be tuned in real time by varying the refractive index of the solution around the NPs.[8]

Hierarchical plasmonic structures show unique optical properties because of the short-range nature of LSPs and the long-range nature of surface plasmon polaritons.[18−20] Multiple waveguide modes with narrow resonances were observed in one-dimensional (1D) nanowire superlattices incorporating both nanowire periodicity and patch periodicity.[21] In addition, for NP superlattices composed of assemblies of synthesized NP building blocks, the volume fraction of both the metal and the dielectric materials in the superlattice influenced the effective permittivity of the assembly and optical properties.[22,23] Besides three-dimensional (3D) NP superlattices made by bottom-up bioprogrammable DNA assembly,[24] two-dimensional (2D) NP superlattices can be fabricated by top-down methods such as electron-beam lithography and photolithography, where finite arrays of NPs (patches) are grouped into larger arrays.[20,25] Despite this hierarchical architecture, the spectral mismatch of the LSPs of the NPs and Bragg modes from patch periodicity did not show evidence of coupling.[25] Also, limited overall patterned areas from e-beam lithography (100 × 100 μm^2) only resulted in broad optical resonances (fwhm > 50 nm).

Multiscale patterning combining photolithography and soft nanolithography can generate superlattices of nanoholes over cm^2 areas, with control over hole size and periodicity as well as patch periodicity.[19,20,26] Hierarchical NP arrays can also be created using the nanohole films as physical deposition masks. With the reported method,[19,20] however, photoresist posts at the center and edges of patches were not equally exposed to UV light because of light scattering at the edge of the Cr mask patches during contact photolithography. Thus, the fabricated NPs were not uniform in size from the patch center to edge, which might preclude the possibility of narrow lattice plasmon resonances.

Here we report superlattice plasmons that can be supported in hierarchical Au NP arrays. To produce NP superlattices with uniform particle sizes, we developed a multiscale nanofabrication approach. We observed multiple narrow superlattice plasmon resonances in 2D arrays of NP patches. To confirm that the origin of the multiple resonances was from the patch periodicity, we fabricated 1D NP patches and characterized their orientation-dependent transmission properties. Moreover, we identified the specific Bragg modes that contributed to the superlattice resonances by simulating both far-field transmission and near-field properties. Similar to lattice plasmons in infinite NP arrays that are defined by NP LSP and NP periodicity, we

Received: September 23, 2015
Published: November 24, 2015

DOI: 10.1021/acsphotonics.5b00546
ACS Photonics 2015, 2, 1789−1794

found that the superlattice plasmons in hierarchical NP arrays can be attributed to coupling of single-patch lattice plasmons with the high-order Bragg modes of the microscale patch periodicity. Finally, we demonstrated that the resonance position and the number of dominant modes of superlattice plasmons can be tuned by varying the patch periodicity and overall patch size.

RESULTS AND DISCUSSION

Hierarchical Au NP arrays on glass were fabricated with multiscale patterning starting with a soft nanofabrication procedure referred to as PEEL (photolithography, etching, electron-beam deposition, and lift-off).[27−29] Briefly, hierarchical photoresist posts on Si wafers were generated by contact photolithography, Cr deposition, resist lift-off, and phase-shifting photolithography with a PDMS mask[30] (Figure 1).

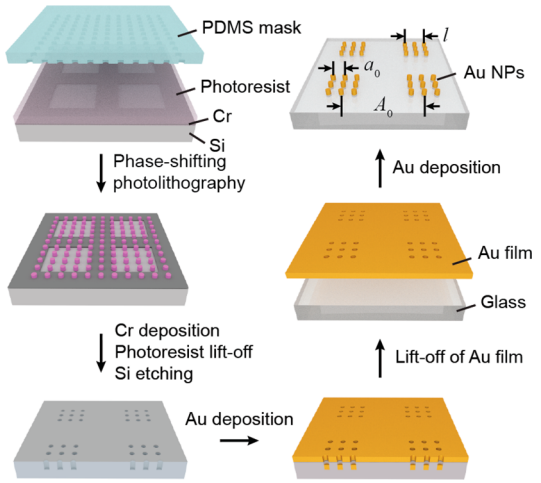

Figure 1. Scheme of the multiscale patterning technique. Typical NP periodicity a_0 = 600 nm, patch side length l = 6 μm, and patch periodicity A_0 = 9 μm.

Here, Cr was used as an isolation layer to create uniform photoresist posts within the patch. Hierarchical patterns of photoresist posts were then transferred into free-standing Au films of hierarchical nanohole arrays by PEEL. Finally, Au deposition through the hole-array mask on glass substrates and then removal of the mask resulted in hierarchical Au NP arrays. Multiscale patterning for generating hierarchical NP arrays has two key advantages: (1) the uniform exposure of UV light ensures that the photoresist posts are homogeneous from patch center to edge; and (2) the Cr masks and PDMS masks can be independently selected to control the patch periodicity A_0, patch side length l, and NP periodicity a_0. The PDMS mask determined the submicron NP periodicity a_0, and the Cr mask determined the microscale patch length l and patch periodicity A_0.

The transmission spectra of hierarchical Au NP arrays were characterized in an index-matched environment consisting of an oil superstrate (n = 1.52) that matched the glass. With the inclusion of microscale patch periodicity in hierarchical arrays, more high-order Bragg modes fell within the resonance envelope of metal LSP to form multiple lattice plasmons with narrow resonances. To determine the influence of patch periodicity on the lattice plasmon resonances, we compared the resonance position of hierarchical NP arrays to that of an infinite NP array. For infinite NP arrays with NP periodicity a_0 = 600 nm and NP diameters d = 140 nm, we observed a single lattice plasmon mode at λ_L = 903 nm (Figure 2a).

For 2D hierarchical NP arrays with the same NP characteristics but with l = 6 μm and A_0 = 9 μm, however, two narrow resonances appeared (Figure 2b). The shorter-wavelength superlattice resonance at λ_{SL} = 904 nm had nearly the same position and fwhm width (15 nm) as the lattice plasmon λ_L in the infinite NP array. The longer-wavelength superlattice resonance appeared at λ_{SL} = 954 nm, with a narrower fwhm of 7 nm. As observed in both infinite and hierarchical arrays, the broad resonance λ_{LSP} around 730 nm was the LSP of a single Au NP, and the Rayleigh anomaly peak λ_{RA} around 630 nm was from coupling with higher-order Bragg modes (Figure 2a).

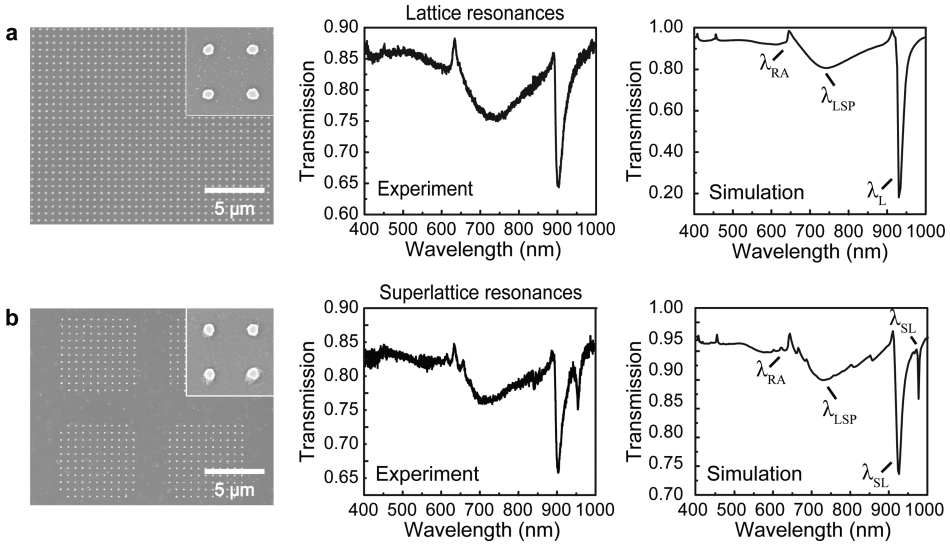

Figure 2. Comparison of transmission spectra between infinite arrays and 2D hierarchical Au NP arrays. (a) SEM images of an infinite NP array with NP periodicity a_0 = 600 nm and NP diameters d around 140 nm. Linear optical properties from experiments and FDTD simulations (n = 1.52) are in excellent agreement. (b) SEM images of 2D hierarchical NP arrays with a_0 = 600 nm, patch side length l = 6 μm, patch periodicity A_0 = 9 μm, and NP d = 140 nm. Linear optical properties from experiment and simulations (n = 1.52) are in excellent agreement.

DOI: 10.1021/acsphotonics.5b00546
ACS Photonics 2015, 2, 1789−1794

Finite-difference time-domain (FDTD) simulations were in good agreement with experiments (Methods). The small shift between simulated and experimental resonance wavelengths can be explained in part by the dispersive properties of the immersion oil used for index-matching (Supporting Information, Figure S1).

To confirm that the multiple resonances were from patch periodicity, we characterized the orientation-dependent transmission properties of 1D NP patches (Figure 3a). These 1D

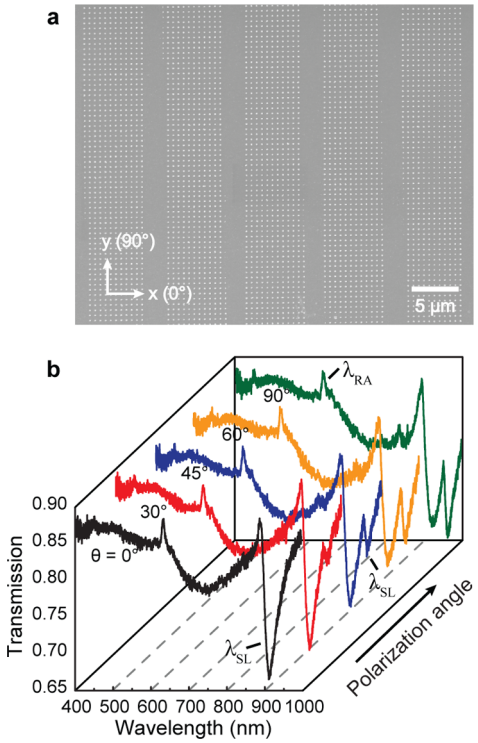

Figure 3. Orientation-dependent transmission properties of 1D Au NP patches. (a) SEM image of fabricated 1D Au NP patches on top of glass, with patch side length l = 6 μm, patch periodicity A_0 = 9 μm along x and NP diameter d = 160 nm. (b) Evolution of transmission spectrum with increasing polarization angle θ from 0° (x direction) to 90° (y direction). The resonance at λ_{SL} = 913 nm maintained its location and amplitude, but the resonance at λ_{SL} = 958 nm gradually emerged and increased in intensity, which indicated that the latter originated from patch periodicity.

patches had the same a_0, l, and A_0 as the 2D hierarchical arrays, but where A_0 was defined only along the x-direction. This symmetry-breaking structure shows polarization-dependent optical properties and different coupling along the x and y directions. To observe the evolution of the transmission spectra with respect to polarization angle more clearly, we fabricated NPs with larger diameters d = 160 nm that showed stronger longer-wavelength resonances (Supporting Information, Figure S2). With the incident light polarized along x, the individual NPs exhibited dipolar oscillations also along x (Supporting Information, Figure S3). The NPs aligned perpendicular to the oscillation direction coupled strongly with each other. Since only NP periodicity a_0 existed along y, the transmission spectrum showed a single narrow lattice plasmon resonance, similar to that of infinite NP array (Figure 3b). As the polarization angle θ increased from 0° (x) to 90° (y), the narrow resonance at λ_{SL} = 913 nm maintained its location and amplitude but a new resonance (λ_{SL} = 958 nm) gradually emerged and increased in intensity. The broad resonance around 730 nm was the λ_{LSP} from single Au NP, and the peak λ_{RA} around 630 nm was Rayleigh anomaly seen earlier in Figure 2b. Note that both were at fixed wavelengths even as θ changed. The spectral evolution with respect to polarization angle suggests that the infinite-like resonance at λ_{SL} = 913 nm in 1D hierarchical patches and the single lattice plasmon λ_L of the infinite NP array are similar regarding resonance wavelength and intensity. In contrast, the resonance at λ_{SL} = 958 nm in the 1D NP patches, which gradually appeared and kept the same position as θ increased, can be attributed to the patch periodicity A_0.

To demonstrate the influence of patch periodicity on the superlattice plasmon resonances, we simulated far-field transmission spectra for a single Au NP, an isolated Au NP patch, and 2D hierarchical Au NP arrays. The simulations can study resonances from a single NP and patch and eliminate coupling effects from nearby NPs and patches, which cannot be achieved in experiments where the incident light spot (~mm^2) was much larger than the single NP or patch size. Figure 4a shows a broad LSP resonance λ_{LSP} from a single Au NP with diameter d = 160 nm. For a single patch containing 10 × 10 NPs with a_0 = 600 nm and d = 160 nm, consistent with the isolated patch in Figure 2b, a single lattice plasmon resonance was observed at λ_L = 965 nm (fwhm 35.7 nm). The single-patch lattice plasmon arose from the coupling of the metal LSP and the Bragg mode determined by the NP periodicity a_0.

For 2D hierarchical NP arrays with l = 6 μm and A_0 = 9 μm, two narrow resonances were observed at λ_{SL}^{15} = 944 nm and λ_{SL}^{14} = 981 nm, as well as one weak resonance at λ_{SL}^{13} = 1056 nm, whose diffraction peaks were in good agreement with the calculated Bragg modes at the n = 15, 14, and 13 orders from patch periodicity A_0 = 9 μm (at 912, 976, and 1051 nm, respectively). The fwhm of the two dominant lattice plasmons at λ_{SL}^{15} and λ_{SL}^{14} were 19.2 and 3.1 nm, respectively, much narrower than that of the single-patch resonances. Similar to lattice plasmons in infinite arrays from coupling the NP LSP and Bragg mode from NP periodicity a_0, superlattice plasmons in hierarchical arrays can be described by the coupling of single-patch lattice plasmons with high-order Bragg modes determined by the patch periodicity A_0. Two-step coupling was involved in generating superlattice plasmons: (1) NP coupling within a single patch and then (2) patch−patch coupling.

The electric field and charge distribution around NPs at the superlattice plasmon resonances illustrated the influence of patch periodicity A_0 on the near-field NP coupling. For resonances at λ_{SL}^{15} = 944 nm, λ_{SL}^{14} = 981 nm, and λ_{SL}^{13} = 1042 nm, the electric field was localized both around and between NPs but with larger enhancement at the narrower resonance at λ_{SL}^{14} than the other two modes (Figure 4b). Compared to λ_{LSP}, single-patch lattice plasmons λ_L had 10-fold local field peak enhancement, while superlattice plasmons had a 15- and 40-fold enhancement at λ_{SL}^{15} and λ_{SL}^{14}, respectively (Supporting Information, Figure S4). At λ_{SL}^{15} and λ_{SL}^{14}, positive and negative charges were located around the NP surface and distributed along the polarization direction of incident light, indicating a dipolar distribution (Figure 4c). At resonances of λ_{SL}^{15}, λ_{SL}^{14}, and λ_{SL}^{13}, there were 15, 14, and 13 phase oscillations within a single patch, which agreed with the order of the Bragg mode that coupled to single-patch lattice plasmons (Figure 4b). Similarly, at the lattice plasmon resonance in infinite NP arrays with a_0 = 600 nm, exactly 15 overall phase oscillations spanned the same

DOI: 10.1021/acsphotonics.5b00546
ACS Photonics 2015, 2, 1789−1794

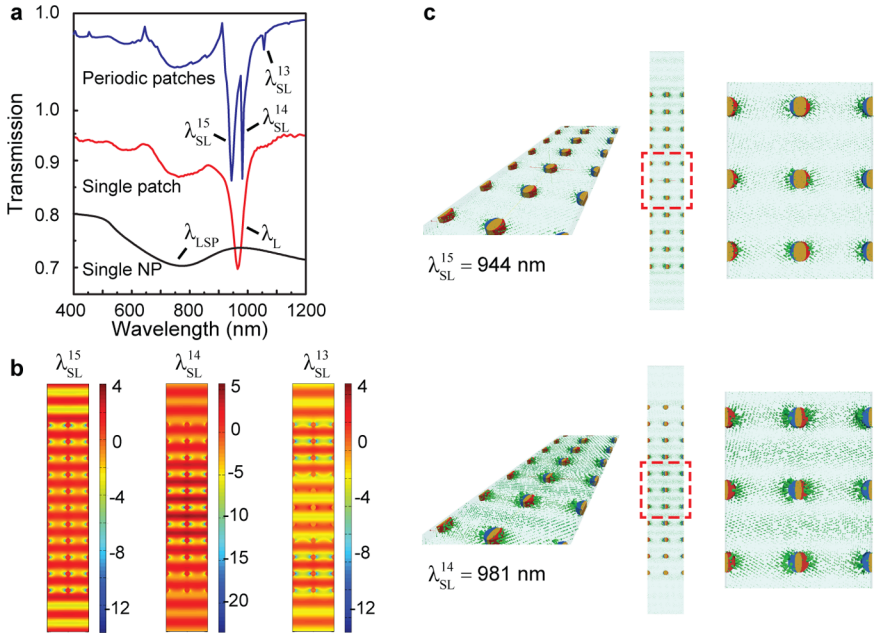

Figure 4. Far-field transmission, near-field electric field, and charge distribution of hierarchical Au NP arrays indicating the origin of superlattice plasmons. (a) Linear optical properties of a single NP, a single patch, and periodic patches with the same NP diameter d = 160 nm, height h = 50 nm, and spacing a_0 = 600 nm. Periodic patches had side length l = 6 μm and periodicity A_0 = 9 μm. (b) Near-field electric field distributions of superlattice plasmons at λ_{SL}^{15} = 944 nm, λ_{SL}^{14} = 981 nm, and λ_{SL}^{13} = 1056 nm within plotted area of 1.2 μm × 9 μm. In simulation, the amplitude of incident plane wave (polarized along x) was set as 1 V/m. The plotted electric field is the real part of E_x with units of V/m. (c) Charge distribution of superlattice plasmons at λ_{SL}^{15} = 944 nm and λ_{SL}^{14} = 981 nm within a plotted area of 1.2 μm × 9 μm.

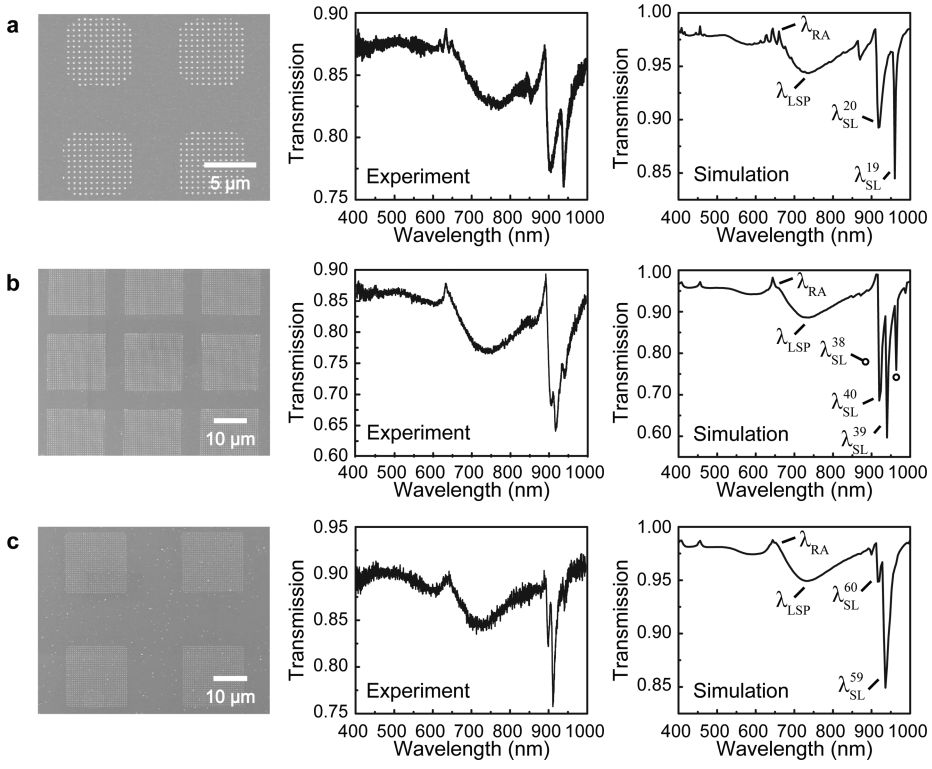

Figure 5. Superlattice plasmons in hierarchical Au NP arrays can be tuned by varying patch periodicity A_0 and side length l. (a) Experimental and simulated linear properties of hierarchical arrays with l = 6 μm, A_0 = 12 μm, and d = 140 nm. (b) Experimental and simulated linear properties of hierarchical arrays with l = 18 μm, A_0 = 24 μm, and d = 140 nm. (c) Experimental and simulated linear properties of hierarchical arrays with l = 18 μm, A_0 = 36 μm, and d = 140 nm.

length scale of patch periodicity (A_0 = 9 μm). Notably, although hierarchical arrays could be viewed as an infinite array with missing NPs, the in-phase oscillation between NPs at infinite-like superlattice plasmon resonance λ_{SL}^{15} was the same as that of lattice plasmon resonance λ_L in infinite arrays. In contrast, the resonance at λ_{SL}^{14} had single-period phase

DOI: 10.1021/acsphotonics.5b00546
ACS Photonics 2015, 2, 1789−1794

oscillations, and the one at λ_{SL}^{13} had two-period phase oscillations between NPs within the single patch. For 1D NP patches at different polarization angles, the in-phase oscillations between NPs were also maintained at λ_{SL}^{15} (θ = 0–90°), while single-period phase oscillations existed at λ_{SL}^{14} (θ > 0°) (Supporting Information, Figure S5).

To illustrate the tunability of superlattice plasmons, we increased A_0 from 9 to 12 μm while keeping patch side length l fixed at 6 μm (Figure 5a). Larger patch periodicity resulted in more high-order Bragg modes with smaller separations and that fell within the resonance envelope of single-patch lattice plasmons. Two dominant lattice plasmon modes at λ_{SL}^{20} = 905 nm and λ_{SL}^{19} = 938 nm were observed, corresponding to the coupling of single-patch lattice plasmons to the n = 20 and 19 orders of Bragg modes from the enlarged patch periodicity A_0 = 12 μm. Compared to the resonances with A_0 = 9 μm (Figure 2b), the shorter-wavelength resonance at λ_{SL}^{20} kept nearly the same position, and the longer-wavelength resonance at λ_{SL}^{19} blue-shifted. At the infinite-like superlattice plasmon resonance λ_{SL}^{20}, where the resonance wavelength and near-field distribution were the same as those of lattice plasmon in infinite arrays, the NPs oscillated in-phase with each other both within an individual patch and between patches (Supporting Information, Figure S6a).

We further increased the number of NPs within one 2D patch from 10 × 10 to 30 × 30 to study the influence of patch side length on superlattice plasmon resonances. Notably, more NPs within one patch created narrower, more intense single-patch lattice plasmons (Supporting Information, Figure S2c). Three dominant lattice plasmon modes at λ_{SL}^{40} = 905 nm, λ_{SL}^{39} = 916 nm, and λ_{SL}^{38} = 939 nm were observed for patch size l = 18 μm and patch periodicity A_0 = 24 μm, corresponding to the coupling of single-patch lattice plasmons to the n = 40, 39, and 38 orders of Bragg modes (Figure 5b). When the patch side length l = 18 μm was maintained and A_0 was increased to 36 μm, we observed one narrow lattice plasmon mode at λ_{SL}^{59} = 911 nm with a fwhm of 2 nm, and a secondary mode at λ_{SL}^{60} = 899 nm (Figure 5c). These two resonances originated from the n = 59 and 60 orders of Bragg modes. The NPs oscillate in-phase with each other at infinite-like resonances of λ_{SL}^{40} (a_0 = 600 nm and A_0 = 24 μm) and λ_{SL}^{60} (a_0 = 600 nm and A_0 = 36 μm; Supporting Information, Figure S6b,c). By varying patch side length l and patch periodicity A_0 in 2D hierarchical arrays, we were able to tune the resonance position and the number of dominant modes for superlattice plasmons.

In summary, we realized superlattice plasmons in hierarchical Au NP arrays. Our multiscale patterning process offers a new approach to generating hierarchical NP arrays over large areas (>cm^2) with independent control over NP periodicity a_0 and patch periodicity A_0. We found that superlattice plasmons could be described by the coupling of the single-patch lattice plasmons to different orders of Bragg modes from the patch periodicity. Hierarchical Au NP arrays showed evidence of coupling between patches. Superlattice plasmon resonances can be manipulated by tuning patch periodicity in addition to NP periodicity. We anticipate that superlattice plasmons, with their ultranarrow resonance line widths and multiple controllable resonant frequencies in the visible region, will be useful in areas such as ultrasensitive sensing as well as energy transfer and plasmon amplification processes in plasmonic cavities.

METHODS

Fabrication of Hierarchical Au NP Arrays. Hierarchical Au NP arrays on glass were fabricated with a multiscale patterning process. A poly(dimethylsiloxane) (PDMS) mask with square lattice periodicity a_0 = 600 nm was used for phase-shifting photolithography to produce photoresist posts with diameter d = 180 and 200 nm. Cr masks with patch features: l = 6 μm, A_0 = 9 μm; l = 6 μm, A_0 = 12 μm), (l = 18 μm, A_0 = 24 μm; and l = 18 μm, A_0 = 32 μm were used for contact photolithography. We used a Cr layer with thickness of 8 nm as a separation layer between phase-shifting and contact photolithography. The hierarchical photoresist posts covered with Cr layer were lifted off with photoresist remover. Deep reactive ion etching (DRIE) was then used to create cylindrical pits through the microscale Cr holes (depth ∼150 nm) inside Si. After depositing ∼90 nm Au and etching the Cr sacrificial layer, a hierarchical Au nanohole array film was produced and floated onto glass substrate. Another deposition of Au and removal of the Au deposition mask resulted in hierarchical Au NPs on glass, with height h = 50 nm and diameters d = 140 or 160 nm.

Linear Optical Property Measurement. A droplet of immersion oil (n = 1.52) was deposited on NP array-glass samples and sandwiched with another piece of cover glass. The samples were then illuminated by collimated white light from a halogen lamp (100 W) with a spot size of 2 mm (Supporting Information, Figure S7). A PIXIS: 400 CCD detector was placed at the backside of sample stage to collect the transmitted light. Data was processed by a Princeton Instruments Acton SP2500 spectrometer. Background light without the sample was taken as a reference to get the transmission spectrum.

Finite Difference Time Domain (FDTD) Simulations. We used FDTD calculations based on a commercial software (FDTD Solutions, Lumerical Inc.) to simulate the linear optical properties of hierarchical Au NP arrays. A uniform mesh size of 4 nm was used in x, y, and z directions. The optical constants of gold were from Johnson and Christy[31] (400–1000 nm). The cylindrical NPs had height h = 50 nm and diameter d = 140 or 160 nm.

ASSOCIATED CONTENT

Supporting Information

The Supporting Information is available free of charge on the ACS Publications website at DOI: 10.1021/acsphotonics.5b00546.

Dispersion property of immersion oil; parameters that influence superlattice plasmon properties; dipolar distribution of 1D NP patches; local field enhancement of superlattice plasmons; near-field distribution of 1D NP patches; near-field distribution of 2D hierarchical NP arrays; linear optical property measurements (PDF).

AUTHOR INFORMATION

Corresponding Authors

*E-mail: todom@northwestern.edu.
*E-mail: g-schatz@northwestern.edu.

Notes

The authors declare no competing financial interest.

ACKNOWLEDGMENTS

This work was supported by the National Science Foundation (NSF) under DMR-1306514 (D.W., G.C.S., T.W.O.). This

DOI: 10.1021/acsphotonics.5b00546
ACS Photonics 2015, 2, 1789–1794

research was conducted with Government support under FA9550-11-C-0028 (A.J.H) and awarded by Department of Defense, Air Force Office of Scientific Research, National Defense Science and Engineering Graduate (NDSEG) Fellowship, 32 CFR 168a. This work made use of the Northwestern University Micro/Nano Fabrication Facility (NUFAB), which is supported by the State of Illinois and Northwestern University and Northwestern University's Atomic and Nanoscale Characterization Experimental Center (NUANCE) Center facilities, which are supported by NSF-MRSEC and the MRSEC (DMR-1121262). This research was supported in part by the Quest high performance computing facility at Northwestern University, which is jointly supported by the Office of the Provost, the Office for Research, and Northwestern University Information Technology.

REFERENCES

(1) Humphrey, A. D.; Barnes, W. L. Plasmonic surface lattice resonances on arrays of different lattice symmetry. *Phys. Rev. B: Condens. Matter Mater. Phys.* **2014**, *90*, 075404.
(2) Kravets, V. G.; Schedin, F.; Grigorenko, A. N. Extremely narrow plasmon resonances based on diffraction coupling of localized plasmons in arrays of metallic nanoparticles. *Phys. Rev. Lett.* **2008**, *101*, 087403.
(3) Chu, Y. Z.; Schonbrun, E.; Yang, T.; Crozier, K. B. Experimental observation of narrow surface plasmon resonances in gold nanoparticle arrays. *Appl. Phys. Lett.* **2008**, *93*, 181108.
(4) Auguie, B.; Barnes, W. L. Collective resonances in gold nanoparticle arrays. *Phys. Rev. Lett.* **2008**, *101*, 143902.
(5) Hicks, E. M.; Zou, S.; Schatz, G. C.; Spears, K. G.; Van Duyne, R. P.; Gunnarsson, L.; Rindzevicius, T.; Kasemo, B.; Kall, M. Controlling plasmon line shapes through diffractive coupling in linear arrays of cylindrical nanoparticles fabricated by electron beam lithography. *Nano Lett.* **2005**, *5*, 1065−1070.
(6) Zou, S.; Schatz, G. C. Narrow plasmonic/photonic extinction and scattering line shapes for one and two dimensional silver nanoparticle arrays. *J. Chem. Phys.* **2004**, *121*, 12606−12612.
(7) Zou, S.; Janel, N.; Schatz, G. C. Silver nanoparticle array structures that produce remarkably narrow plasmon lineshapes. *J. Chem. Phys.* **2004**, *120*, 10871−10875.
(8) Yang, A.; Hoang, T. B.; Dridi, M.; Deeb, C.; Mikkelsen, M. H.; Schatz, G. C.; Odom, T. W. Real-time tunable lasing from plasmonic nanocavity arrays. *Nat. Commun.* **2015**, *6*, 6939.
(9) Vakevainen, A. I.; Moerland, R. J.; Rekola, H. T.; Eskelinen, A. P.; Martikainen, J. P.; Kim, D. H.; Torma, P. Plasmonic surface lattice resonances at the strong coupling regime. *Nano Lett.* **2014**, *14*, 1721−1727.
(10) Schokker, A. H.; Koenderink, A. F. Lasing at the band edges of plasmonic lattices. *Phys. Rev. B: Condens. Matter Mater. Phys.* **2014**, *90*, 155452.
(11) Zhou, W.; Dridi, M.; Suh, J. Y.; Kim, C. H.; Co, D. T.; Wasielewski, M. R.; Schatz, G. C.; Odom, T. W. Lasing action in strongly coupled plasmonic nanocavity arrays. *Nat. Nanotechnol.* **2013**, *8*, 506−511.
(12) Vazquez-Mena, O.; Sannomiya, T.; Villanueva, L. G.; Voros, J.; Brugger, J. Metallic nanodot arrays by stencil lithography for plasmonic biosensing applications. *ACS Nano* **2011**, *5*, 844−853.
(13) Kuznetsov, A. I.; Evlyukhin, A. B.; Goncalves, M. R.; Reinhardt, C.; Koroleva, A.; Arnedillo, M. L.; Kiyan, R.; Marti, O.; Chichkov, B. N. Laser fabrication of large-scale nanoparticle arrays for sensing applications. *ACS Nano* **2011**, *5*, 4843−4849.
(14) Auguie, B.; Bendana, X. M.; Barnes, W. L.; de Abajo, F. J. G. Diffractive arrays of gold nanoparticles near an interface: Critical role of the substrate. *Phys. Rev. B: Condens. Matter Mater. Phys.* **2010**, *82*, 155447.
(15) Auguie, B.; Barnes, W. L. Diffractive coupling in gold nanoparticle arrays and the effect of disorder. *Opt. Lett.* **2009**, *34*, 401−403.
(16) Anker, J. N.; Hall, W. P.; Lyandres, O.; Shah, N. C.; Zhao, J.; Van Duyne, R. P. Biosensing with plasmonic nanosensors. *Nat. Mater.* **2008**, *7*, 442−453.
(17) Thackray, B. D.; Kravets, V. G.; Schedin, F.; Auton, G.; Thomas, P. A.; Grigorenko, A. N. Narrow Collective Plasmon Resonances in Nanostructure Arrays Observed at Normal Light Incidence for Simplified Sensing in Asymmetric Air and Water Environments. *ACS Photonics* **2014**, *1*, 1116−1126.
(18) Kichin, G.; Weiss, T.; Gao, H.; Henzie, J.; Odom, T. W.; Tikhodeev, S. G.; Giessen, H. Metal-dielectric photonic crystal superlattice: 1D and 2D models and empty lattice approximation. *Phys. B* **2012**, *407*, 4037−4042.
(19) Odom, T. W.; Gao, H. W.; McMahon, J. M.; Henzie, J.; Schatz, G. C. Plasmonic superlattices: Hierarchical subwavelength hole arrays. *Chem. Phys. Lett.* **2009**, *483*, 187−192.
(20) Henzie, J.; Lee, M. H.; Odom, T. W. Multiscale patterning of plasmonic metamaterials. *Nat. Nanotechnol.* **2007**, *2*, 549−554.
(21) Zentgraf, T.; Christ, A.; Kuhl, J.; Gippius, N. A.; Tikhodeev, S. G.; Nau, D.; Giessen, H. Metallodielectric photonic crystal superlattices: Influence of periodic defects on transmission properties. *Phys. Rev. B: Condens. Matter Mater. Phys.* **2006**, *73*, 115103.
(22) Young, K. L.; Ross, M. B.; Blaber, M. G.; Rycenga, M.; Jones, M. R.; Zhang, C.; Senesi, A. J.; Lee, B.; Schatz, G. C.; Mirkin, C. A. Using DNA to design plasmonic metamaterials with tunable optical properties. *Adv. Mater.* **2014**, *26*, 653−659.
(23) Ross, M. B.; Ku, J. C.; Vaccarezza, V. M.; Schatz, G. C.; Mirkin, C. A. Nanoscale form dictates mesoscale function in plasmonic DNA-nanoparticle superlattices. *Nat. Nanotechnol.* **2015**, *10*, 453−458.
(24) Macfarlane, R. J.; Lee, B.; Jones, M. R.; Harris, N.; Schatz, G. C.; Mirkin, C. A. Nanoparticle superlattice engineering with DNA. *Science* **2011**, *334*, 204−208.
(25) Sung, J.; Hicks, E. M.; Van Duyne, R. P.; Spears, K. G. Nanoparticle spectroscopy: Plasmon coupling in finite-sized two-dimensional arrays of cylindrical silver nanoparticles. *J. Phys. Chem. C* **2008**, *112*, 4091−4096.
(26) Gao, H. W.; Hyun, J. K.; Lee, M. H.; Yang, J. C.; Lauhon, L. J.; Odom, T. W. Broadband Plasmonic Microlenses Based on Patches of Nanoholes. *Nano Lett.* **2010**, *10*, 4111−4116.
(27) Henzie, J.; Kwak, E. S.; Odom, T. W. Mesoscale metallic pyramids with nanoscale tips. *Nano Lett.* **2005**, *5*, 1199−1202.
(28) Gao, H.; Henzie, J.; Odom, T. W. Direct evidence for surface plasmon-mediated enhanced light transmission through metallic nanohole arrays. *Nano Lett.* **2006**, *6*, 2104−2108.
(29) Henzie, J.; Barton, J. E.; Stender, C. L.; Odom, T. W. Large-area nanoscale patterning: Chemistry meets fabrication. *Acc. Chem. Res.* **2006**, *39*, 249−257.
(30) Odom, T. W.; Love, J. C.; Wolfe, D. B.; Paul, K. E.; Whitesides, G. M. Improved pattern transfer in soft lithography using composite stamps. *Langmuir* **2002**, *18*, 5314−5320.
(31) Johnson, P. B.; Christy, R. W. Optical Constants of Noble Metals. *Phys. Rev. B: Condens. Matter Mater. Phys.* **1972**, *6*, 4370−4379.

DOI: 10.1021/acsphotonics.5b00546
ACS Photonics 2015, 2, 1789−1794